

Mechanisms of radiation damage to Sc/Si multilayer mirrors under EUV laser irradiation

Y P Pershyn¹, E N Zubarev¹, D L Voronov^{1,4}, V A Sevryukova¹,
V V Kondratenko¹, G Vaschenko^{2,5}, M Grisham², C S Menoni²,
J J Rocca², I A Artioukov³, Y A Uspenskii³ and A V Vinogradov³

¹ Metal and Semiconductor Physics Department, National Technical University 'Kharkiv Polytechnic Institute', Frunze Street 21, Kharkiv 61002, Ukraine

² NSF ERC for Extreme Ultraviolet Science and Technology and Department of Electrical and Computer Engineering, Colorado State University, Fort Collins, CO 80523, USA

³ P N Lebedev Physical Institute, Moscow 117942, Russia

E-mail: persh@kpi.kharkov.ua

Received 13 February 2009, in final form 28 April 2009

Published 4 June 2009

Online at stacks.iop.org/JPhysD/42/125407

Abstract

Specific structural changes in Sc/Si multilayer mirrors irradiated with extreme ultraviolet (EUV) laser single pulses ($\lambda = 46.9$ nm) at near damage threshold fluences (0.04–0.23 J cm⁻²) are analysed. We have identified melting of surface layers as the basic degradation mechanism for the mirrors. Both heat generation during silicide formation and low heat conduction of the layered system significantly decreases the degradation threshold of Sc/Si multilayer mirrors compared with bulk materials. The results are relevant to the use of the multilayer mirrors for shaping and directing the intense beams produced by the new generation of coherent EUV sources.

1. Introduction

The development of high-reflectance extreme ultraviolet (EUV) and x-ray multilayer (ML) optics ($1 < \lambda < 70$ nm) has provided a successful solution of many basic and applied problems related to efficient manipulation of EUV beams. However, recent progress in EUV/x-ray sources of a new generation, e.g. free electron lasers (FEL) [1, 2] and compact capillary-discharge lasers [3, 4], as well as synchrotron facilities [5] creates a new challenge in applications of ML optics.

Most of the earlier studies on the degradation of optical properties and the structural modification of the ML EUV/x-ray mirrors were conducted mainly for the thermal influence. These studies can be considered as reference background since any irradiation treatment of materials is always accompanied by heating. They also provide the ML

survival temperature and help in distinguishing thermal effects from pure radiation-induced ones [6]. A large number of experimental investigations have been dedicated to this subject [7–13], with some works focusing on the study of degradation mechanisms [14–19] and others on different techniques for increasing thermal stability of the MLs [20–23].

The resistance of the ML mirrors to intense EUV/x-ray radiation has not been studied in such detail. The first efforts in this direction were made for hard x-rays in connection with the development of a facility to filter white synchrotron light [24] and the construction of a diagnostic instrument to characterize high-intensity sources [25]. Both conventional MLs such as W/C, W/B₄C, W/Si, Mo/B₄C, Mo/Si [6, 26–29] and specially proposed ones (Mo/BN, W/BN [30]) were tested. It was demonstrated that synchrotron light at power densities of ~ 0.4 W mm⁻² can warm the ML surface beyond 440 °C [26]. A correlation in ML stability between thermal and radiation tests was noticed [30]: more thermally stable MLs had higher radiation stability. Depending on the ML, the degradation is observed at power densities of 0.25–2.30 W mm⁻² [6, 26, 30] for synchrotron light and at fluences ranging from 0.05 [27] up

⁴ Currently with Lawrence Berkeley National Laboratory, ALS Division, Berkeley, CA, USA

⁵ Currently with Cymer, Inc., San Diego, CA, USA.

to 0.46 [25] J cm⁻² for pulsed light. The degradation manifests itself in a shift or broadening of the reflecting maximum, decay of the reflectivity or their combination. Previous results also include the measurement of reflectivity dynamics for various MLs under x-ray plasma irradiation [27–29] exhibiting the ML performance stability on a picosecond timescale. The role of graphitization in the damage of carbon-based MLs is emphasized [7, 28, 31]. The degradation mechanisms suggested to be the reason for optical degradation are reactive diffusion of layers [26] and phase transformation within the individual layers [28].

This decade new results concerning interaction of femtosecond-pulse light from FEL with matter are published. They are connected mainly with irreversible changes induced at the surfaces of metals, semiconductors and insulators both in bulk and thin-film states [32] to be used as materials for total reflection optics [33]. Different surface morphology modifications similar to those for visible laser (e.g. laser-induced periodic surface structure [33]) but with finer features [34] are observed. There is also some evidence of non-thermal ablation during EUV irradiation of insulators [35]. Damage fluences for different materials in the range of 0.03–0.14 J cm⁻² are evaluated [32, 36]. It is also shown both theoretically and experimentally that single-pulse damage threshold for homogeneous materials is comparable to their thermal melt threshold [32].

Recently Mo/Si [37] and Si/C [38] MLs have been shown to keep their reflectivity under a FEL single-pulse irradiation on the timescale of ~30 fs even at fluences higher than their damage thresholds. The damage fluences of ~0.3 J cm⁻² observed for the Si/C ML [38] are comparable to those for the component materials [32, 36]. In the irradiated region the layers recrystallize and interdiffuse. The damage is local in character and snaps the irradiated ML volume only.

Although the information on radiation stability and potentialities of ML optics is substantial, it is necessary to supply it with accompanying structural studies, which are very important for understanding the mechanisms of the damage [29]. At present, structural studies of rationally damaged ML optics are practically absent. Mechanisms and thresholds of irradiation damage for many types of widely used ML mirrors and a variety of EUV/x-ray sources also remain to be studied, as well as methods to increase their radiation stability.

Herein we report results of studying the near-threshold damage (0.06–0.23 J cm⁻²) in Sc/Si ML mirrors irradiated with intense EUV laser pulses of nanosecond duration at 46.9 nm wavelength. Until now Sc/Si-based ML mirrors have the highest reflectivity in the wavelength range of 35–50 nm [39]. These types of mirrors were developed specifically [40] to manipulate the EUV beam from the pulsed Ne-like Ar capillary-discharge lasers [3, 4]. The high pulse energy of these lasers has been successfully utilized for the study of the reflectivity of Sc/Si ML mirrors, and, using a focused beam, for the ablation of materials [41, 42]. In our recent letter [43, 44] we reported on the damage threshold in Sc/Si mirrors under irradiation with the EUV laser. In this paper we expand the discussion on the damage mechanisms in Sc/Si ML mirrors

based on the results of a detailed investigation of the structural changes in the irradiated mirrors. As in the case of the previous work, we take advantage of the unique characteristics of the capillary-discharge laser, which is at this point one of the brightest laser sources operating at 46.9 nm [45].

2. Sample preparation and experimental methods

The Sc/Si ML samples were fabricated using dc magnetron sputtering by alternate deposition of Sc and Si layers onto substrates of polished Si wafers and borosilicate glass (RMS roughness $\sigma \sim 0.4$ –0.6 nm). The number of periods is 33. The ML coatings had a period of ~27 nm that corresponds to a maximum reflectance for 46.9 nm radiation at normal incidence. The Sc-containing layer occupies approximately half of the period. Each ML coating is capped with a 7 nm thick Si layer to protect the ML coating from oxidation. In the as-deposited state the Sc/Si ML constitutes a periodic structure consisting of alternate layers of amorphous silicon (a-Si) and polycrystalline scandium (c-Sc) separated by amorphous interlayers of mixed Sc and Si. These interlayers are typically formed as a result of the interdiffusion of Sc and Si during the deposition process [46]. Interlayers have a composition and a density close to equiatomic silicide ScSi [46]. The reflectivity of the ML sample deposited on glass substrates studied in this work was measured to be ~30% at 46.9 nm.

The Sc/Si ML samples were irradiated by focused EUV pulses from a 46.9 nm capillary-discharge Ne-like Ar laser operating at a repetition rate of 1 Hz. Each pulse exposed a different region of the sample surface. The laser was set to operate with an energy of ~0.13 mJ in a pulse, whereas the pulse duration was ~1.2 ns. The far-field laser beam profile has an annular shape with a peak-to-peak divergence of about 4.6 mrad [3]. Because of this intensity distribution hereinafter we shall utilize mean values of fluences except for the cases where accounting for the exact beam shape is important. The shot-to-shot variation of the laser intensity is ~15%.

The beam was focused onto flat ML samples with dimensions of ~3 × 7 mm² by a Sc/Si ML mirror deposited onto a spherical substrate (the reflectivity $R \sim 35\%$ at 46.9 nm). The samples were mounted on a brass sample holder attached to a motorized XYZ translation stage (figure 1). The focusing mirror was located behind the sample, approximately 1.45 m from the exit of the laser. Thus the sample and the holder were shadowing a small portion of the laser beam that had a diameter of 13 mm in this location. The advantage of this configuration is that it allows the laser beam to be focused onto the sample at normal incidence, minimizing the aberrations introduced by the focusing mirror. The laser fluence on the sample surface could be varied within the range 0.01–10.00 J cm⁻² by changing the position of the sample with respect to the focal spot along the laser beam axis. For irradiation of a large area (~2 × 2 mm²) the sample position was continuously scanned in the direction normal to the beam while the laser was running at 1 Hz.

The irradiated samples were studied using scanning electron microscopy (SEM), transmission electron microscopy (TEM), selected-area electron diffraction (SAED) and x-ray

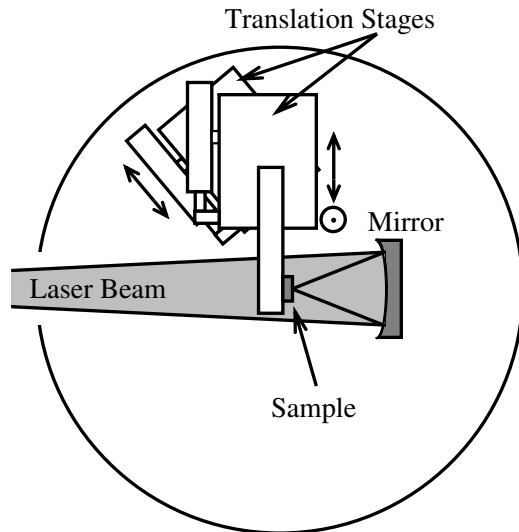


Figure 1. Schematic diagram of the experimental setup used for the irradiation of the samples with 46.9 nm pulses from a Ne-like Ar capillary-discharge laser.

reflectivity techniques. The images of the surface patterns of the irradiated MLs were taken with a JEOL JSM-820 scanning electron microscope. The cross-sectional images of the layered structure and interfaces were obtained with a transmission electron microscope PEM-U (SEMI, Ukraine) at an accelerating voltage of 100 kV with point-by-point resolution of better than 0.3 nm. The procedures used in the preparation of the cross-sections of the samples are similar to those described in [47, 48]. Briefly, we started with mechanical thinning followed by ion etching. Xe⁺-ions with an energy of 4.5 keV were used at the first stage of etching and then at the final stage the ion energy was decreased down to 2 keV for fine etching. The temperature of the samples did not exceed $T = 100^\circ\text{C}$ during all stages. Separately, for in-plane TEM, Si/Sc/Si three-layer films were prepared with layer thicknesses similar to those in the ML samples. Subsequently, such coatings were detached from the substrate using a standard technique and attached onto a microscopic grid. In this state they were exposed to the focused EUV radiation.

X-ray reflectivity at $\lambda = 0.154\text{ nm}$ was used to define the characteristics of both the as-grown and the irradiated ML samples. The measurements were made with a diffractometer DRON-3M (NPO 'Burevestnik', Russia) assembled as a double-crystal spectrometer with a (220) Si monochromator. Processing of the resulting reflection curves allowed us to determine the ML period with an accuracy better than 0.2%.

For the detailed study of processes taking place in the Sc/Si MLs at low fluences ($F < 0.3\text{ J cm}^{-2}$) corresponding to near-threshold conditions, we prepared special samples with an irradiated area of $\sim 2 \times 2\text{ mm}^2$ (figure 2(a)). Preparation of such samples allowed us also to conduct x-ray studies and substantially facilitated the preparation of the cross-sectional specimens for transmission electron microscopy.

3. Results

3.1. Scanning electron microscopy

Figure 2 shows the scanning electron microscopy (SEM) images of four samples irradiated with mean EUV fluences of $\sim 0.23\text{ J cm}^{-2}$ (sample #1), $\sim 0.10\text{ J cm}^{-2}$ (#2), $\sim 0.08\text{ J cm}^{-2}$ (#3) and $\sim 0.04\text{ J cm}^{-2}$ (#4). These fluences correspond to single laser imprints with nominal diameters of $\sim 160\text{ }\mu\text{m}$, $\sim 240\text{ }\mu\text{m}$, $\sim 310\text{ }\mu\text{m}$ and $\sim 400\text{ }\mu\text{m}$, respectively. Figure 2 also demonstrates uniform irradiation coverage in a relatively large area ($2 \times 2\text{ mm}^2$), which was possible due to the high pulse energy and high repetition rate of the EUV laser. To the best of our knowledge, such large area surface modification with coherent EUV radiation has never been done before.

A sample irradiated with a fluence of 0.23 J cm^{-2} is shown in figures 2(a) and (b). SEM images of the irradiated area reveal the formation of a visible surface roughness and a net of cracks, which are commonly observed in molten surfaces. The central unexposed area of a rectangular shape (figure 2(b)) is formed by the shadow of the sample and the sample holder (see figure 1 and [42]). Reducing the fluence down to $\sim 0.10\text{ J cm}^{-2}$ leads to a reduction in the portion of the molten area within the laser imprint (figure 2(c)). The molten area reproduces the annular shape of the focused laser beam with a $50\text{--}60\text{ }\mu\text{m}$ wide ring. At the periphery of the laser imprint a $4\text{--}16\text{ }\mu\text{m}$ wide area of apparent discoloration is also revealed in the images obtained with secondary electrons. It can be speculated that the ML coating in this area was subjected to heating, although the temperature did not reach the level required for melting. At the irradiation fluence of $\sim 0.08\text{ J cm}^{-2}$ the portion of the molten area further decreases (figure 2(d)). Reducing the fluence to $\sim 0.04\text{ J cm}^{-2}$ results in discoloration of only negligible small spots, whereas the overall area of the noticeable damage in the Sc/Si ML coating is less than 3% (figure 2(f)). We therefore conclude that the damage threshold for melting of the investigated MLs is $\sim 0.08\text{ J cm}^{-2}$.

We note here that the discoloration was observed only in the images obtained with secondary electrons (sampling depth $\sim 10\text{ nm}$) (figure 2(e) top), and not with reflected electrons (sampling depth $\sim 300\text{ nm}$) (figure 2(e) bottom). This finding suggests that only a narrow, less than one period, surface layer is modified upon irradiation of the ML coating at these fluences.

The results for the irradiated samples shown in figure 2 are summarized in table 1. The last column of the table describes characteristic features of the damage for each fluence. For sample #1 the melting (always followed by cracking) is a dominating mechanism of the ML degradation. As the fluence is reduced, the beam inhomogeneity starts to manifest itself in an appearance of discoloured areas (heated below melting temperature) coexisting with the areas of molten material. Further reduction of the fluence leads to the gradual reduction of the molten area portion; while the portion of the discoloured area increases and becomes largest (samples #2 and #3). In sample #4 we see only traces of the irradiation damage associated with fluence fluctuations. Since table 1 gives only mean values of the fluence within the laser imprint, we assume that in the absence of fluctuations the damage traces in sample #4 most likely would not appear. Indeed, our estimations

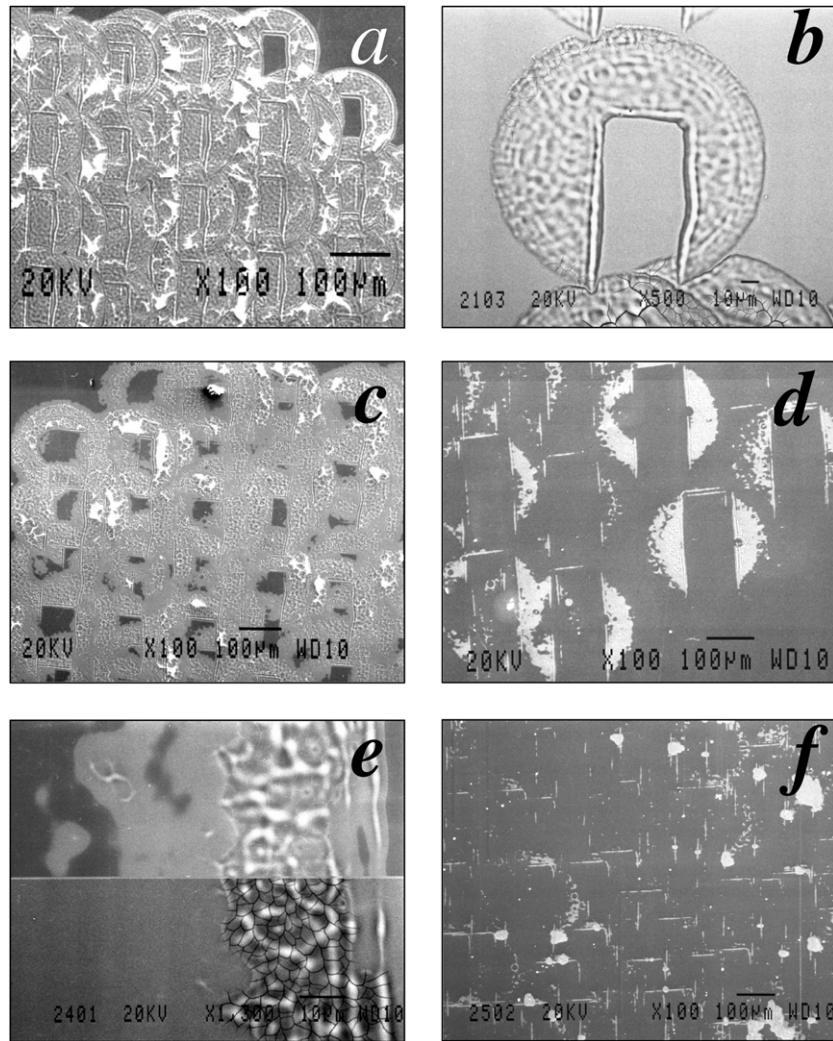


Figure 2. SEM images of the Sc/Si MLs irradiated with $\lambda = 46.9$ nm laser emission: (a) and (b) fluence of 0.23 J cm^{-2} ; (c) 0.10 J cm^{-2} ; (d) and (e) 0.08 J cm^{-2} ; (f) 0.04 J cm^{-2} .

Table 1. Damage parameters in large area ($2 \times 2 \text{ mm}^2$) irradiation Sc/Si MLs.

Sample number	Fluence (J cm^{-2})	Laser spot diameter (nominal) (μm)	Mean imprint diameter (observed) (μm)	Ring width (μm)	Discoloration region width (μm)	Character of the damage
1	0.23	160	157	75–80	—	Melting Cracking
2	0.10	240	244	50–60	4–16	Flaking Melting Cracking
3	0.08	310	264	30–50	28–58	Discoloration Discoloration Melting
4	~ 0.04	400	NA	3–5	0–102	Cracking Discoloration Melting (traces) Cracking (traces)

suggest that the surface of sample #2 melts roughly in the middle of the laser pulse duration, whereas the surface of sample #3 is expected to melt only by the very end of the pulse (in our estimation we neglected the heat removal from the surface).

3.2. X-ray reflectometry ($\lambda = 0.154 \text{ nm}$)

X-ray reflectivity spectra revealed features typical for the MLs in all the exposed samples. Figure 3 illustrates two such spectra for samples #1 and #2 subjected to fluences of 0.23

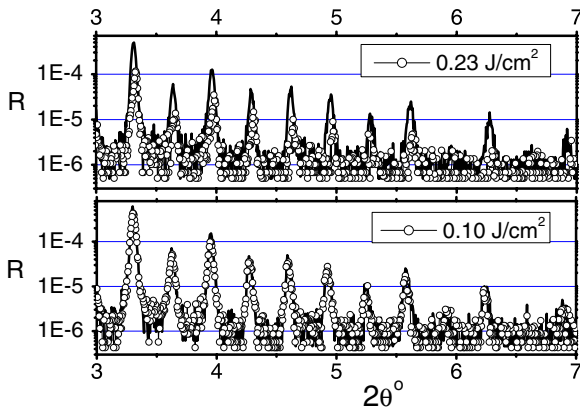


Figure 3. X-ray reflectivity spectra (circles) measured in sample #1 (irradiation fluence $\sim 0.23 \text{ J cm}^{-2}$) (a) and in sample #2 (irradiation fluence $\sim 0.10 \text{ J cm}^{-2}$) (b). Spectra for the as-deposited samples are shown by solid lines.

(This figure is in colour only in the electronic version)

(figure 2(a)) and 0.10 J cm^{-2} (figure 2(c)). The reflectivity spectra are shown only for the angles $2\theta > 3^\circ$ since at smaller angles the 0.05 mm wide x-ray beam catches the undamaged sample area outside the $2 \times 2 \text{ mm}^2$ irradiated spot. As can be seen from figure 3 the angle positions of each Bragg maxima for irradiated samples coincide with those for the same samples in the as-deposited state. However, the peak intensities dropped noticeably compared with the initial state. Thus, for example, at the EUV fluence of $\sim 0.23 \text{ J cm}^{-2}$ the peak intensity reductions are 75–85%, whereas at 0.10 J cm^{-2} they are only 20–35%. The reflectivities of Bragg maxima in the as-deposited state and after irradiation do not differ significantly ($\pm 1\%$) at lower fluences. These experimental observations indicate that only the top portion of the ML coating is typically molten as the result of irradiation with EUV beam. The rest of the structure does not undergo noticeable changes. The ratio of Bragg intensities measured before and after irradiation provides information about the thickness of the molten layer. Our estimates based on this parameter result in an average molten layer thickness of $350 \pm 70 \text{ nm}$ (or 16 ± 3 periods) for sample #1 and $88 \pm 40 \text{ nm}$ (or 4 ± 2 periods) for sample #2. In these calculations we assumed uniform irradiation coverage of the entire surface of the samples and that the alloy in the molten layer has a composition close to Sc_3Si_5 silicide (close to the nominal atomic ratio of Sc and Si).

3.3. Transmission electron microscopy

3.3.1. Three-layer samples. To analyse the phase transformations in the irradiated MLs at near-threshold fluences we investigated samples composed of three layers: Si(27.0 nm)/Sc(13.5 nm)/Si(13.5 nm). Such thin-film structures have sufficient transparency for the electron microscopy and compared with MLs supported by a substrate are better suited for selecting and visualizing areas with a certain type of damage over the large field of the sample. The three-layer structures supported by a copper grid were exposed to the EUV fluence of $\sim 0.10 \text{ J cm}^{-2}$, which resulted in the formation of through holes in the samples. The hole

formation is associated with melting, rolling up due to surface tension and mechanical separation, rather than laser ablation. Outside the holes the fluence is gradually decaying below the melting threshold. In this region one can see essential changes in the structure and the phase composition of the three-layer. The electron microscopy (figures 4(a) and (c)) and SAED (figure 4(b)) show that the amorphous silicon (a-Si) and the crystalline scandium (c-Sc) found in the as-deposited state are transformed into crystalline silicide $\text{c-Sc}_3\text{Si}_5$ (with grain dimension of 100–150 nm) and c-Si (figure 4(a)). We observe this structure over a distance of $\sim 18 \mu\text{m}$ from the hole edge. As we move further away from the edge an additional $\sim 2 \mu\text{m}$, the structure and phase changes occur in the following order: $\text{c-Sc}_3\text{Si}_5 + \text{c-Si} \rightarrow \text{c-Sc}_3\text{Si}_5 + \text{a-Si} \rightarrow \text{c-Sc} + \text{a-Si}$ (figures 4(a) and (c)). As the c-Si phase disappears the grain size reduces to 50–100 nm. This is consistent with a lowering of the temperature of the material. At $\sim 20 \mu\text{m}$ from the hole edge the silicide lines in the SAED disappear, and c-Sc lines appear instead. Beyond $\sim 20 \mu\text{m}$ the three-layer again consists of c-Sc (grain size of 5–10 nm) and a-Si as in the as-deposited state.

These structural and phase transformations, ending in a transition to the as-grown state as we move away from the hole edge, are closely related to the reduction of the local laser fluence towards the beam periphery and the corresponding reduction in temperature. Based on the results of the analysis in this section we can suggest that one of the stages in the Sc/Si ML degradation process under the EUV laser irradiation may be an interlayer diffusion interaction [46] resulting in silicide formation which proceeds in a solid state.

3.3.2. Cross-sections of the ML samples. Cross-sectional TEM images of the Sc/Si ML mirrors irradiated at the fluence of $\sim 0.1 \text{ J cm}^{-2}$ (figure 5(a)) reveal two distinct zones: a molten zone (MZ) at the top of the ML and a layered zone near the substrate. The thickness of the MZ is $\sim 280 \text{ nm}$ (figure 5(a)) and the number of layered periods is 19 (out of 33 in the as-deposited state). It is worth noting that the MZ thickness varies quite substantially across the irradiated area of the ML. Thus, within $\sim 10 \mu\text{m}$ of the field shown in figure 5(a), the MZ thickness varies from ~ 170 up to $\sim 530 \text{ nm}$. This variation is the effect of radial non-uniformity of the irradiating beam. The MZ thickness revealed here with the TEM is significantly larger than that estimated in section 3.2 with x-rays for the same sample (#2). The reason for this difference is that with TEM we are imaging only a small segment of the sample, whereas the x-ray diffraction provides an averaged signal for the entire irradiated area.

According to SAED measurements, the MZ represents an alloy of $\text{c-Sc}_3\text{Si}_5$ and c-Si. From the nominal ratio of components, we estimate that the chemical interaction of components during the formation of the Sc_3Si_5 silicide should result in complete consumption of Sc with minor excess of Si. Using large-scale cross-section images of the ML structures (figure 5(a)), we evaluated the shrinkage of the coating in the MZ. It was found that there was a decrease of 20–26 vol% on average, which is in good agreement with the value expected in the studied ML coating due to the formation of Sc_3Si_5 . This also suggests that at $\sim 0.1 \text{ J cm}^{-2}$ of irradiation fluence there

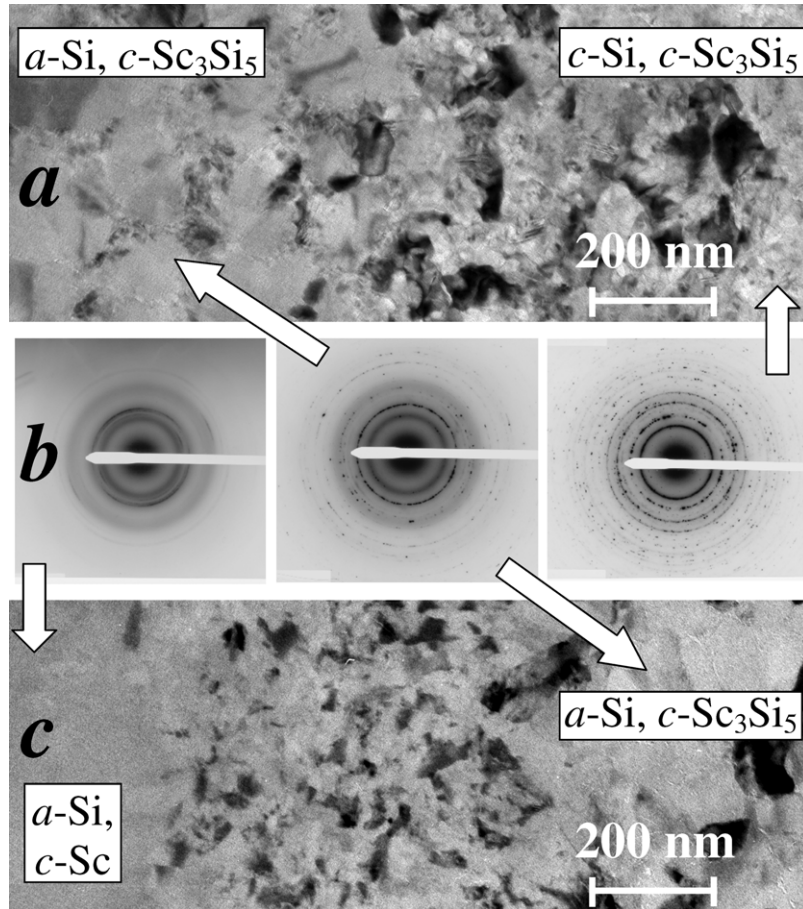


Figure 4. In-plane TEM images (*a*) and (*c*) and the corresponding selected-area electron diffractions (*b*) for free-standing Si(27.0 nm)/Sc(13.5 nm)/Si(13.5 nm) three-layers near a hole made by focused EUV laser radiation with fluence of $\sim 0.10 \text{ J cm}^{-2}$.

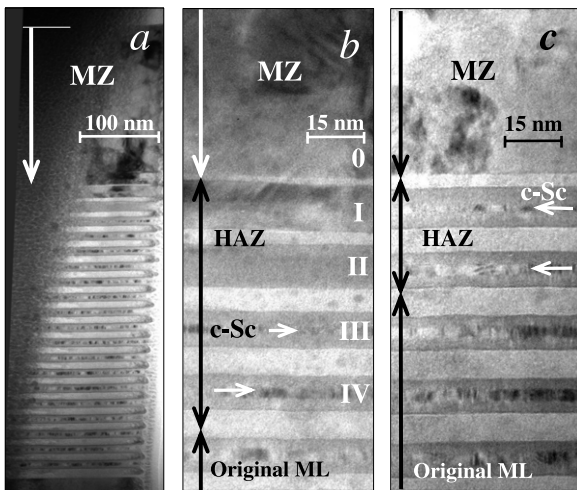


Figure 5. Cross-sectional TEM images of sample #2 showing general view (*a*) and the smaller regions of the mirror around the HAZ with 14 (*b*) and 25 (*c*) damaged periods.

is no noticeable evaporation of the coating material from the surface.

Detailed analysis of the TEM images also reveals another region, a part of the layered zone that is confined between the molten and unchanged zones: a heat-affected zone [49] (HAZ) (figures 5(*b*) and (*c*)). Within this zone, a few layers differ by

thickness and structure from the rest of the layers in the layered zone. Thus, in the area with 19 unchanged periods shown in figure 5(*b*) the HAZ has four periods with Sc-containing layers indicated by Roman numerals from I to IV. We observe here that the ScSi interlayers in the Sc-containing layers III and IV became only slightly thicker, whereas the Sc-containing layers I and II are noticeably widened, and the pure c-Sc layer disappears.

It is also interesting to note that the number of layers involved in the HAZ correlates inversely with the thickness of the MZ. We have found that in the MLs where only a small number of periods is damaged ($N < 8-14$ periods) the HAZ extends over three or four periods (figure 5(*b*)), whereas the structures with a larger thickness of the MZ are characterized by relatively abrupt HAZ (about two periods) with some residual c-Sc layer in the first layer adjacent to the MZ (figure 5(*c*)). The reason for the HAZ thickness increasing from about two periods for a relatively deep MZ (thickness more than $0.5 \mu\text{m}$) up to four periods for a relatively shallow MZ ($< 0.3 \mu\text{m}$) is not clear at present. A possible explanation is that the shallow MZ transmits more EUV light into the underlying layers that are transformed by this emission.

Using the method described earlier [16, 48], we have estimated the consumption of components based on tabulated densities of pure components [50] and silicides [51] to find that the interlayer widening for layers III and IV is at the expense

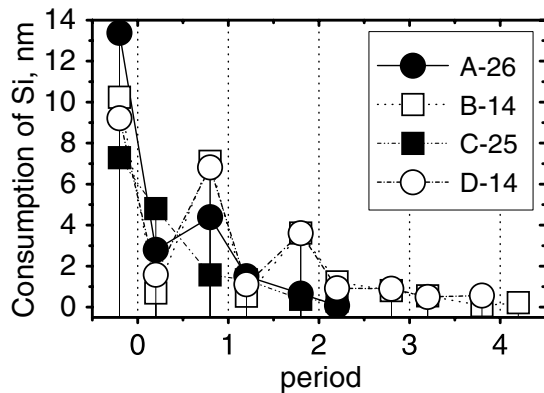


Figure 6. Consumption of silicon at interfaces during diffusion interaction between Sc and Si layers for four regions in sample #2. Images for the regions B-14 and C-25 are shown in figures 5(b) and (c), respectively.

of ScSi silicide formation. Upon the total consumption of c-Sc, as is the case for layers I and II, another silicide Sc_3Si_5 is also formed (calculation suggests ~ 15 vol% of Sc_3Si_5 for layer II and ~ 60 vol% for layer I). The Sc-containing layer I (figure 5(b)) also displays two distinct sublayers: the upper half of the layer is darker than the lower half. Since the ScSi and Sc_3Si_5 silicides have similar densities (3.36 g cm^{-3} and 3.39 g cm^{-3} , respectively), the observed contrast has a diffractive rather than absorptive nature. It means that one of the silicides crystallized, and its crystallites appeared in a reflecting position, thus forming a dark area in the top portion of the layer. We are inclined to ascribe this feature to Sc_3Si_5 because this silicide is expected to appear in the top, higher temperature portion of the layer. This explanation is in agreement with our earlier investigation of the isothermally annealed Sc/Si MLs where formation of a-ScSi silicide and its subsequent transformation into c- Sc_3Si_5 at higher temperatures was observed upon full consumption of Sc-layers [52].

We have also evaluated the consumption of the elemental components in the reaction at each interface separately. We began with the periods where some c-Sc was left (for example, layers III and IV in figure 5(b)). Then using obtained data as well as changes in thickness of both Sc-containing layers and adjoining Si layers, the component consumption within periods containing no traces of c-Sc (layers I and II in figure 5(b)) was defined. Figure 6 shows the results of the evaluation for Si consumption at each interlayer in the HAZ for four different regions of sample #2, namely A-26, B-14, C-25 and D-14. The numbers in the region designations indicate the number of molten periods in the MZ of each region. The values of Sc consumption are not presented here due to their similarity to those for Si. Besides, as we determined earlier for the Sc/Si system [53, 54], silicon is the dominant diffusant. Thus, it is the Si atom activity that governs the diffusion kinetics.

Analysis of figure 6 reveals two features in the behaviour of Si consumption as a function of the interface distance from the MZ: (1) an order of magnitude oscillations near the MZ with an amplitude significantly decaying over 3–4 interfaces and (2) a monotonic decay in the consumption far from the MZ (3–5 interfaces). The oscillating character in the consumption

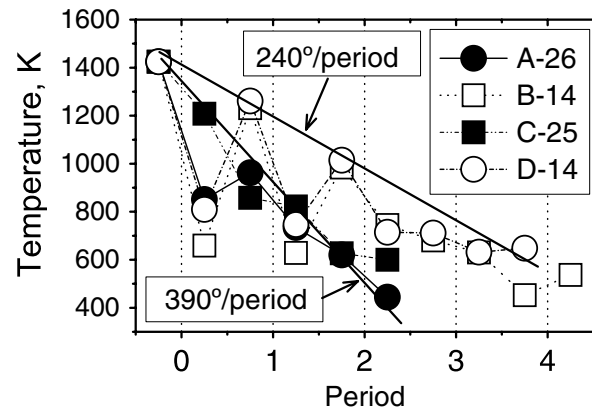


Figure 7. Evaluated temperatures at the interfaces in the HAZ of laser irradiated Sc/Si ML at a fluence of 0.10 J cm^{-2} .

indicates the predominance of Si-diffusion flux through the top Sc interfaces.

We consider that upon irradiation of the ML coating with a laser pulse, a heat wave moving from the top of the ML appears creating a time gradient. As the wave propagates deep into the ML it is decaying due to ML heat capacity and heat removal. Besides, the temperature within each layer, as was shown for nanoscale MLs [55], varies negligibly compared with the temperature drop at the interfaces. These three factors result in a temperature difference between adjacent Sc interfaces on a fast timescale. In the presence of the temperature gradient and due to the finite thickness of Sc layers, the Sc/Si ML system initially transforms to ScSi/Si at the expense of Si atoms preferentially diffusing through the top Sc interface. The gradient of chemical potential which is the driving force for Si-atom diffusion drops, and this decreases the subsequent Si-diffusion flux at both Sc interfaces. As a result the total Si flux through the bottom Sc interface slows down so much that it becomes smaller than the flux at the top Sc interface not only for the given period but also for the next underlying one.

For those periods where some pure Sc is still present after the radiation-induced heating, we observe a monotonic decay in Si consumption (figure 6). Due to the lower temperature in this region of the HAZ the Si diffusion through the top Sc interface is comparatively slow to consume scandium entirely. As a result, the chemical potential gradient for Si atoms diffusing at the bottom interface is close to that for Si atoms diffusing from the top. Under these conditions, only the interface temperature defines the consumption of Si at both interfaces.

As the densities of thin films can differ from the tabulated values, we also estimated possible modifications of dependences shown in figure 6 due to such variations. We have found that the oscillating character of the Si consumption remains unchanged if the densities of only silicides are, for instance, smaller than the tabulated values by as much as 10%, although the amplitude of the oscillations reduces by almost a half. If silicides, Sc and Si densities were off by the same amount, the dependence would remain the same.

We can evaluate the temperature gradient in the HAZ assuming that the diffusion mechanism is the same for all interfaces therein. For the diffusivity being $D \sim (x^2 - x_0^2)/\tau$

(x_0 —initial silicide thickness, x —silicide thickness at certain interface in the HAZ, τ —diffusion time) the diffusion time is cancelled in the ratio of diffusivities at different interfaces and then Si consumption can be used as the measure of the diffusion length. We used activation energy of $\varepsilon_a = 0.57$ eV obtained earlier in our 1 h annealing study of Sc/Si MLs to solve equations set for diffusivity ratios. The estimated temperatures are shown in figure 7 for the case where the temperature at the MZ/HAZ boundary is taken at ~ 1430 K—the temperature of the low-melting eutectic Sc–Si binary alloy system [56]. The temperature gradient is defined using temperature values at the top interfaces mainly (especially in the high-temperature portion) as diffusion here dominates (figure 6). The slope ratio of the lines drawn through the experimental points gives the corresponding temperature gradients (figure 7). We observe mainly two temperature gradients: $\sim 240^\circ$ per period (or $\sim 0.9 \times 10^{10}$ degree m^{-1}) for smaller HAZ (MZ containing ~ 14 periods) and $\sim 390^\circ$ per period (or $\sim 1.4 \times 10^{10}$ degree m^{-1}) for deeper HAZ (MZ of 25–26 periods). These values represent the lower limits of temperature gradients as in the periods of the HAZ, where c-Sc is consumed. The diffusion at the top interfaces is also suppressed due to the finite thickness of the Sc layer, just as it is at the bottom interfaces.

4. Discussion

One of our intentions was to establish a correlation between the fluence value and certain structural changes in the ML samples. In particular, we wanted to know whether there is a basic mechanism of ML degradation for each fluence or whether deterioration of EUV optical properties was connected with the combined effect of several physical processes. In this work we observed three different degradation mechanisms to be considered: (1) melting of surface layers (see sections 3.1, 3.2 and 3.3.2); (2) surface damage within ~ 1 period (section 3.1) and (3) interdiffusion of layers (section 3.3.1). To clarify the contribution of each mechanism we performed model calculations. We assumed that the Sc/Si ML consisted of pure crystalline Sc and crystalline Si with tabulated densities (3.0 g cm^{-3} and 2.3 g cm^{-3} , correspondingly). The portion of scandium, β , in the period was 0.4 (period $d = 10.8 \text{ nm}$ (Sc)+16.2 nm (Si)), which corresponded to a nominal portion of Sc in the samples. With such β the atomic ratio between components is in a proportion close to 3:5. In this initial simulation the presence of ScSi interlayers is not considered yet.

We can calculate the temperature of the individual layers using absorption values given by Henke *et al* [57] and tabulate thermal constants for the bulk materials without heat removal first and then evaluate the amount of heat removal. We took into consideration that $\sim 30\%$ of the incident laser radiation is reflected by the ML sample itself. After two reflections (from the focusing mirror ($\sim 35\%$) and the ML sample) the mean energy of laser radiation absorbed in each ML for one shot is $\sim 3.2 \times 10^{-5}$ J. Most of the EUV laser energy ($>80\%$) that is exponentially decaying in the ML is absorbed within the volume of the top 7 periods. Under this energy the top Si-layer of sample #2 (diameter of laser spot is $\sim 240 \mu\text{m}$)

should be heated up to ~ 2080 K and the Sc layer up to ~ 2400 K, which corresponds to a mean temperature value of ~ 2240 K for the first period. Averaging the temperature over each period we get a mean temperature gradient of $\sim 175^\circ$ per period or $\sim 6 \times 10^9$ degree m^{-1} . Based on the heat conduction equation ($q = -\Lambda \text{grad } T$), we obtain that a heat-flux density, q , with a mean heat-conduction coefficient $\Lambda \sim 20 \text{ W m}^{-1} \text{ K}^{-1}$ (estimated from the tabulated data [50]) amounts to $\sim 1.2 \times 10^{11} \text{ W m}^{-2}$, i.e. for a time of ~ 1.2 ns (time being comparable to the laser pulse duration) only an energy of $\sim 5.6 \times 10^{-6}$ J, or less than 20% of all absorbed laser energy, can be removed from the irradiated volume by the heat conduction. This percentage is practically the same (does not exceed 25%) for the intensities across the EUV laser beam. This means that even in the presence of the heat removal our crude estimations of temperatures remain relevant.

The calculation also indicates that within the laser spot of sample #2 ($F \sim 0.1 \text{ J cm}^{-2}$) only the two top periods could melt. As a result of energy fluctuation across the laser beam this value can reach a maximum of up to 4 periods. In the hypothetical case where all absorbed energy is released at the ML subsurface only, it may melt at most the 8 top periods. However, experimentally observed MZ spans up to 26 periods, that is at least three times as large as the most favourable prediction. This discrepancy can be understood if we consider two effects described in the following.

First. An additional thermal energy can arise due to the reaction of silicide formation in Sc–Si binary system [58, 59]. For example, the enthalpy of the reaction $\text{Sc} + \text{Si} = \text{ScSi}$ is $\nabla H^0 \sim -87 \text{ kJ mol}^{-1}$ [58]. Taking into account entropy [58] the Gibbs free energy at 1430 K reduces to $\sim -70 \text{ kJ mol}^{-1}$. This energy ($\sim 2.4 \times 10^{-6}$ J) is sufficient to heat up and melt the volume by itself (in addition to the laser heating) and it is comparable to the energy absorbed in each of the top periods. It is known from the previous work [60] that diffusivities of silicon in liquid metals can reach $D \sim 10^{-4} - 10^{-5} \text{ cm}^2 \text{ s}^{-1}$. With such diffusivities all the silicon atoms should diffuse into the Sc layers with the formation of ScSi within $\sim 3 - 30$ ns, correspondingly. This also defines the minimal time scale for heat release during silicide formation. Taking into account that the laser pulse can melt top layers of the ML in a shorter time, it is possible that the reaction and the heat release run in a liquid state.

Second. Let us evaluate the heat removal at the melt boundary deep into the ML sample. Thermal gradient in the HAZ can be as high as $\sim 10^{10}$ degree m^{-1} (see section 3.3.2). Assuming $\Lambda \sim 20 \text{ W m}^{-1} \text{ K}^{-1}$ we find that all energy released during silicide formation in the 4 top periods ($\sim 10^{-6}$ J) should be removed deep into the ML for ~ 1 ns. This means that either we should not observe the melting of ML deeper than 4 periods or the released heat is not removed so fast. It is known that both metals [61, 62] and semiconductors [63–65] in thin-film configuration can have significantly lower heat conduction compared with bulk materials. Furthermore, as was shown for superlattices [55, 66] and for metallic MLs [67] with layer thickness on the same scale as the Sc/Si MLs investigated here, the heat conduction can be reduced by an order of magnitude compared with the bulk value. Comparing the evaluation of

heat removal time in the HAZ with the characteristic diffusion time, we can conclude that the mean heat conduction of the studied samples takes about one-tenth of the bulk, and its average value is $\sim 2 \text{ W m}^{-1} \text{ K}^{-1}$ or even less. This is perhaps one of the main reasons for the low damage threshold in Sc/Si MLs compared with bulk silicon [43].

It is worth noting that the heat generated by the EUV light does not spread much beyond the illuminated spot. The maximum expansion of the MZ in depth, as shown above experimentally, is $\sim 0.7 \mu\text{m}$ (or 26 periods). So the appearance of discolored areas at the periphery of the irradiated spot (figure 2(e)), which extends up to $16 \mu\text{m}$ (see table 1), is the direct result of laser exposure and not the expansion of the HAZ.

Thus, the process of heating the ML at fluences exceeding the melting threshold ($F > 0.08 \text{ J cm}^{-2}$) should pass through the following stages: (1) heating the ML surface up to a melting temperature without essential modification of the layered structure; (2) melting of the individual layers and their interdiffusion; (3) silicide formation, heat release and heating the sample and (4) subsequent heating and melting of deeper regions. Upon the melting and intermixing of the layers, heat conduction of the relatively homogeneous liquid increases compared with the layered region, and temperature within the melt homogenizes. As the MZ expands further, due to the difference in the heat conduction of the liquid and the ML the energy released in the reaction in the new regions is mainly confined to the molten state. The melt temperature, which reaches a maximum value in the few surface periods melted by the laser, decreases gradually due to the heat removal. At some point, as the molten material cools down and crystallizes, the cooling rate of the MZ slows down near the crystallization temperature. The HAZ is formed during this transition.

The second mechanism of degradation (surface damage within ~ 1 period, visible in SEM pictures as discoloration) can be explained by the sublimation of surface oxide. It is well known [68] that a 1.5–3.0 nm layer of SiO_{2-x} is formed on the surface of a a-Si film exposed to atmosphere. Due to the high absorption of EUV light at $\lambda = 46.9 \text{ nm}$ by oxygen, this thin passivating layer receives more than twice as much energy as the first ML period. Our estimates show that in sample #2 the absorbed energy is sufficient to warm the oxide layer up to a boiling temperature ($T_b = 3223 \text{ K}$) [69]. However, as it is reported in [70], at $\sim 1500 \text{ K}$ SiO_2 has a noticeable evaporation rate. Our estimation shows that sublimation of the oxide film can occur at $F \geq 0.01 \text{ J cm}^{-2}$, i.e. for all the samples studied. This is consistent with the experimental observations (see figure 2 and table 1). Due to possible fluctuations in the structure of the oxide layer, its composition, its thickness and the density over the surface, it can evaporate non-uniformly. So we associate the appearance of discolorations in the SEM images (figure 2) with a roughening of the ML surface, which the secondary electrons in SEM are sensitive to (section 3.1).

In our experiments diffusion as a result of direct influence of the laser radiation is quite well observed in the three-layer samples (section 3.3.1). Here the heat removal is lower by a factor of $\sim 10^3$ than that in the MLs on a substrate since it is possible along the layers only. The diffusion in the ML depends

on the heat conduction of the layered matter and diffusive mobility of atoms, i.e. on the ratio of the values of heat removal and total energy of both the absorbed energy (from laser) and the heat released in the reaction. Under favourable conditions, for instance, temperatures below the melting one with $D \sim 10^{-6} \text{ cm}^2 \text{ s}^{-1}$ and $\Lambda \sim 0.1 \text{ W m}^{-1} \text{ K}^{-1}$ when temporal scales of diffusion and heat removal are comparable (at microsecond rate), interdiffusion can be observed at cross-sections of MLs. This situation could likely be realized in samples #3 and #4 within 1–2 surface periods where the temperature of Sc can rise to $\sim 1000 \text{ K}$. Although due to a drop of absorbed energy deep into the ML and the exponential dependence of D on temperature, the diffusion should cease in deeper periods. In the cases of $D \sim 10^{-7} \text{ cm}^2 \text{ s}^{-1}$ or $\Lambda \sim 1 \text{ W m}^{-1} \text{ K}^{-1}$ the diffusion interaction is most likely not important.

Considering now the non-ideal Sc/Si MLs, the presence of ScSi interlayers leads, on the one hand, to a lower heat generation due to a smaller amount of interacting materials. This should shift the onset of the noticeable diffusion processes up into the region of the melt temperatures. On the other hand, the increased number of interfaces per one ML period should additionally reduce the ML heat conduction. The latter, in our opinion, plays the key role in melting the ML region deeper than 8 periods due to the low heat removal. In other words ScSi interlayers should make the heat effects described above more pronounced.

It is worth noting that a superposition of successive laser shots visible in figure 2 does not substantially affect the damage pattern as a consequence of ‘additive effect’. Fluences lower than or comparable to that for the original exposure do not change the damage area (as visible in figure 2(b)) since the primary heat release should already be over, and the laser energy is not localized any more at the ML surface due to low heat conductivity of the layered surface. In the case of a significant overlap of two exposed areas, where the second exposure has a higher fluence, the effect of the first exposure is a minor contribution to the damage produced by the following laser pulse.

Thus, the melting of ML surface under the influence of laser pulses for $F \geq 0.08 \text{ J cm}^{-2}$ is the main mechanism of mirror degradation that is accompanied by the interdiffusion. Sublimation of the SiO_{2-x} layer takes place at all EUV fluences used in this work, although this event cannot be considered as a degradation in a full sense, as the reflectivity can rise after oxide removal. Excessive accumulation of heat in the SiO_{2-x} layer, however, may also facilitate the triggering of the exothermic reaction of silicide formation from the top Si–Sc interface.

5. Conclusions

In this work we studied the damage mechanisms of Sc/Si ML mirrors irradiated with intense nanosecond EUV single pulses from a capillary-discharge laser operating at 46.9 nm. The study is based on detailed microscopic and macroscopic analysis of the layer structure in the MLs irradiated with laser fluences in the 0.04–0.23 J cm^{-2} range. Melting of subsurface layers at the laser fluences $F \geq 0.08 \text{ J cm}^{-2}$ is found to be the basic mechanism of mirror degradation. This fluence threshold

is an order of magnitude lower than the similar threshold value for single-crystal Si wafer [44]. Exothermic reaction of Sc and Si leading to silicide formation is a significant source of additional heat that increases the damaged volume of Sc/Si ML at least six fold with respect to that directly caused by the EUV laser irradiation. Layered matter of the samples has decreased heat conduction compared with the values for pure bulk materials. As a result, a significant heat accumulation takes place in the irradiated ML surface. Heat generation and low heat conduction are the two main factors leading to the dramatic reduction of threshold fluences for ML samples, which is in good agreement with our earlier study [43].

Interdiffusion of layers in the HAZ underneath the molten layers necessarily associated with melting is an accompanying mechanism of degradation. We did not observe evidence of solid-phase interdiffusion in the layers of Sc and Si as a result of direct laser irradiation.

At fluences of $0.08 \leq F \leq 0.23 \text{ J cm}^{-2}$ three different stacked zones can be discerned within the volume of Sc/Si ML mirrors: (1) a zone of entirely molten matter consisting mainly of Sc_3Si_5 silicide at the surface of the ML, (2) a HAZ with partially reacted layers; the layer structure in this zone successively changes from (c- Sc_3Si_5 +ScSi)/a-Si near the MZ to a-ScSi/c-Sc/a-ScSi/a-Si and (3) a zone retaining the initial ML structure. The thickness of the HAZ amounts to $\sim 0.05\text{--}0.10 \mu\text{m}$ or 2–4 ML periods. The phase composition in the different zones of the irradiated Sc/Si ML resembles that in the Sc/Si MLs after 1 h annealing in 400–800 K temperature range [52].

We observed the inverse correlation between the thickness of the MZ and the thickness of the HAZ: the larger HAZs (spanning ~ 4 periods) were found under smaller ($< 0.3 \mu\text{m}$) MZs, whereas the smallest HAZs (≤ 2 periods) were observed under large ($> 0.5 \mu\text{m}$) MZs. The temperature gradients in the HAZs were estimated to be $\sim 1 \times 10^{10} \text{ degree m}^{-1}$.

Large temperature gradients between adjacent interfaces in the HAZs, which are arising dynamically under irradiation, and the finite layer thicknesses lead to an asymmetric consumption of Si in Sc–Si solid-state reaction, with Si diffusing predominately through the top Sc interfaces. As a result, Si consumption as a function of interface location has an oscillating character.

The high degree of phase and structural non-equilibrium of the layered Sc/Si system makes it rather sensitive to irradiation. Suppressing the interlayer interaction can increase the damage threshold. This can be accomplished, for instance, by adding diffusion barrier layers at the Sc–Si and Si–Sc interfaces. The viability of this technique has already been demonstrated [71–73] which resulted in the significant improvement of thermal stability. Alternatively, the interlayer diffusion interaction can also be suppressed by using equilibrium materials [19], namely Sc_3Si_5 (in place of c-Sc) and Si. The use of these techniques is expected to improve the radiation stability of the Sc/Si ML mirrors, although additional studies are required to assess the effect of these changes on the reflectivity of such mirrors.

Acknowledgments

The authors would like to thank Professor A T Pugachev and Dr V V Zorchenko for useful advice and discussion of results. This work was supported by the US Department of Energy, Chemical Sciences, Geosciences and Biosciences Division of the Office of Basic Energy Sciences, and in part by the Engineering Research Centers Program of the National Science Foundation under NSF Award Number EEC-0310717. The authors also acknowledge the support of the US Civilian Research and Development Foundation and the W M Keck Foundation. This publication is based on the work supported by Award No RUP2-2845-MO-06 of the US Civilian Research & Development Foundation (CRDF).

References

- [1] Ayvazyan V *et al* 2006 *Eur. Phys. J. D* **37** 297
- [2] Ackermann W *et al* 2007 *Nat. Photon.* **1** 336
- [3] Benware B R, Macchietto C D, Moreno C H and Rocca J J 1998 *Phys. Rev. Lett.* **81** 5804
- [4] Macchietto C D, Benware B R and Rocca J J 1999 *Opt. Lett.* **24** 1115
- [5] Bilderback D H, Elleaume P and Weckert E 2005 *J. Phys. B: At. Mol. Opt. Phys.* **38** S773
- [6] Kortright J B, Joksich S and Ziegler E 1991 *J. Appl. Phys.* **69** 168
- [7] Jiang Z, Jiang X, Liu W and Wu Z 1989 *J. Appl. Phys.* **65** 196
- [8] Jankowski A F, Schrawyer L R and Wall M A 1990 *J. Appl. Phys.* **68** 5162
- [9] Dupuis V, Ravet M F, Tête C, Piecuch M, Lepetre Y, Rivoira R and Ziegler E 1990 *J. Appl. Phys.* **68** 5146
- [10] Jergel M, Holý V, Majkova E, Luby S and Senderak R 1997 *J. Appl. Crystallogr.* **30** 642
- [11] Veldkamp M, Zabel H, Schäfers F and Mertins H-Ch 1998 *J. Appl. Phys.* **84** 3147
- [12] Bugaev E A, Zubarev E N, Kondratenko V V, Penkov A V, Pershin Yu P and Fedorenko A I 1999 *Surf. Investigation* **15** 141
- [13] Wang W-H, Bai H Y, Zhang M, Zhao J H, Zhang X Y and Wang W K 1999 *Phys. Rev. B* **59** 10811
- [14] Ziegler E, Lepetre Y, Schuller I K and Spiller E 1986 *Appl. Phys. Lett.* **48** 1354
- [15] Krawietz R, Wehner B, Meyer D, Richter K, Mai H, Dietsch R, Hopfe S, Scholz R and Pompe W 1995 *Fresenius J. Anal. Chem.* **353** 246
- [16] Holloway K and Sinclair R 1988 *J. Less-Common Metals* **140** 139
- [17] Stearns D G, Stearns M B, Cheng Y, Stith J H and Ceglio N M 1990 *J. Appl. Phys.* **67** 2415
- [18] Kopilets I A, Kondratenko V V, Fedorenko A I, Zubarev E N, Poltseva O V, Ponomarenko A G and Lyakhovskaya I I 1996 *J. X-ray Sci. Technol.* **6** 141
- [19] Bugaev E A, Fedorenko A I, Kondratenko V V and Zubarev E N 1995 *J. X-ray Sci. Technol.* **5** 295
- [20] Kondratenko V V, Fedorenko A I, Pershin Y P, Zubarev E N, Yulin S A, Kozhevnikov I V, Sagitov S I, Chirkov V A, Levashov V E and Vinogradov A V 1993 *Appl. Opt.* **32** 1811
- [21] Takenaka H, Kawamura T and Ishii Y 1995 *J. Appl. Phys.* **78** 5227
- [22] Takenaka H and Kawamura T 1996 *J. Electron Spectrosc. Relat. Phenom.* **80** 381
- [23] Ishino M, Yoda O, Sano K and Koike M 2002 *Proc. SPIE* **4782** 277
- [24] Kortright J B, Plag P, Perera R C C, Cowan P L, Lindle D W and Karlin B 1988 *Nucl. Instrum. Methods Phys. Res. A* **266** 452

- [25] Kohler D, Guttman J L and Watson B A 1985 *Rev. Sci. Instrum.* **56** 812
- [26] Ziegler E, Lepetre Y, Joksich S, Saile V, Mourikis S, Viccaro P J, Rolland G and Laugier F 1989 *Rev. Sci. Instrum.* **60** 1999
- [27] Le Guern F et al 1996 *Rev. Sci. Instrum.* **67** 2107
- [28] MacGowan B J, Mrowka S, Barbee T W Jr, DaSilva L B, Eder D C, Koch J A, Pan L S, Turner J A, Underwood J H and Young P E 1993 *J. X-ray Sci. Technol.* **3** 231
- [29] Leguern F, Andre J-M, Lebreton J-P, Dutrannoy J-L, Chauvineau J-P, Krastev K, Larcade J-L, Friart D, Nazet C and Barchewitz R 1997 *J. X-ray Sci. Technol.* **7** 271
- [30] Yanagihara M, Mayama K, Goto Y, Kusunoki I, Asaoka S and Maezawa H 1993 *Nucl. Instrum. Methods Phys. Res. A* **334** 638
- [31] Gonzales-Hernandez J, Chao B S, Pawlik D A, Allred D D and Wang Q 1992 *J. Vac. Sci. Technol. A* **10** 145
- [32] Hau-Riege S P et al 2007 *Appl. Phys. Lett.* **90** 173128
- [33] Steeg B, Juha L, Feldhaus J, Jacobi S, Sobierajski R, Michaelsen C, Andrejczuk A and Krzywinski J 2004 *Appl. Phys. Lett.* **84** 657
- [34] Pelka J B, Andrejczuk A, Reniewicz H, Schell N, Krzywinski J, Sobierajski R, Wawro A, Zytkeiwicz Z R, Klinger D and Juha L 2004 *J. Alloys Compounds* **382** 264
- [35] Juha L et al 2005 *J. Electron Spectrosc. Relat. Phenom.* **144–147** 929
- [36] Krzywinski J et al 2004 *Proc. 2004 FEL Conf. (Trieste)* p 675
- [37] Chapman H N et al 2006 *Nature Phys.* **2** 839
- [38] Hau-Riege S P et al 2007 *Phys. Rev. Lett.* **98** 145502
- [39] Uspenskii Yu A, Levashov V E, Vinogradov A V, Fedorenko A I, Kondratenko V V, Pershin Yu P, Zubarev E N and Fedotov V Yu 1998 *Opt. Lett.* **23** 771
- [40] Vinogradov A V 2002 *Quantum Electron.* **32** 1113
- [41] Artyukov I A, Benware B R, Vinogradov A V, Kas'yanov Yu S, Kondratenko V V, Macchietto K D, Ozols A, Rocca J J and Chilla J L A 2000 *Quantum Electron.* **30** 328
- [42] Benware B R, Ozols A, Rocca J J, Artiukov I A, Kondratenko V V and Vinogradov A V 1999 *Opt. Lett.* **24** 1714
- [43] Grisham M, Vaschenko G, Menoni C S, Rocca J J, Pershyn Yu P, Zubarev E N, Sevryukova V A, Kondratenko V V, Vinogradov A V and Artiukov I A 2004 *Opt. Lett.* **29** 620
- [44] Voronov D L et al 2007 *Proc. SPIE* **6702** 67020U
- [45] Vinogradov A V and Rocca J J 2003 *Quantum Electron.* **33** 7
- [46] Fedorenko A I, Pershin Yu P, Poltseva O V, Ponomarenko A G, Sevryukova V A, Voronov D L and Zubarev E N 2001 *J. X-ray Sci. Technol.* **9** 35
- [47] Bravman J C and Sinclair R 1984 *J. Electron Microsc. Tech.* **1** 53
- [48] Yulin S, Feigl T, Kuhlmann T, Kaiser N, Fedorenko A I, Kondratenko V V, Poltseva O V, Sevryukova V A, Zolotarev A Yu and Zubarev E N 2002 *J. Appl. Phys.* **92** 1216
- [49] Luft A, Franz U and Kasper J 1996 *Appl. Phys. A* **63** 93
- [50] Andreeva T V et al 1976 *Physical properties Handbook on Properties of Elements* ed G V Samsonov (Moscow: Metallurgiya) Chapter 1, p 600 (in Russian)
- [51] Alekseev A G et al 1986 *Handbook on Properties, Preparation and Application of Refractory Compounds* ed T Ya Kosolapova (Moscow: Metallurgiya) p 928 (in Russian)
- [52] Voronov D L, Zubarev E N, Kondratenko V V, Penkov A V and Pershin Yu P 2002 *Funct. Mater.* **9** 534
- [53] Voronov D L 2002 *Phase transformation in Sc/Si and Sc/W/Si/W multilayer film systems PhD Thesis* V N Karazin Kharkov National University (in Russian)
- [54] Voronov D L, Zubarev E N, Kondratenko V V, Pershin Yu P, Sevryukova V A and Bugayev Ye A 2006 *Thin Solid Films* **513** 152
- [55] Chen G and Neagu M 1997 *Appl. Phys. Lett.* **71** 2761
- [56] Eremenko V N, Meleshkevich K A and Buyanov Yu I 1988 *Poroshkovaya Metallurgiya (Powder Metallurgy)* vol 12 p 52 (in Russian)
- [57] Henke B L, Gullikson E M and Davis J C 1993 *At. Data Nucl. Data Tables* **54** 181
- [58] Lukashenko G M, Polotskaya R I and Sidorko V R 1992 *J. Alloys Compounds* **179** 299
- [59] Golutvin Yu M, Maslennikova E G and Titov L G 1984 *Izv. Akad. Nauk SSSR Met.* **6** 47
- [60] Lepinskih B M, Kaybichev A V and Savel'ev Yu A 1974 *Diffusion of Elements in Liquid Metals of Iron Series* (Moscow: Nauka) p 191 (in Russian)
- [61] Pugachev A T and Churakova N P 1996 *Mineralogicheskii Zhurnal (Mineral. J.)* **18** 30 (in Russian)
- [62] Kumar S and Vradis G C 1994 *J. Heat Transfer* **116** 28
- [63] Balandin A, Khitun A, Liu J L, Wang K L, Borca-Tasciuc T and Chen G 1999 *18th Conf. Thermoelectrics (Baltimore, MD)* p 189
- [64] Moon S, Hatanabo M, Lee M and Grigoropoulos C P 2002 *Int. J. Mass Heat Transfer* **45** 2439
- [65] Cahill D G, Ford W K, Goodson K E, Mahan G D, Majumdar A, Maris H J, Merlin R and Phillpot S R 2003 *J. Appl. Phys.* **93** 793
- [66] Chen G 1997 *J. Heat Transfer* **119** 220
- [67] Zhng L, Bain J A, Zhu J-G, Abelman L and Onoue T 2006 *Physica B* **381** 204
- [68] Bajt S, Alameda J B, Barbee T W, Miles Clift W, Folta J A, Kaufmann B and Spiller E A 2002 *Opt. Eng.* **41** 1797
- [69] Samsonov G V et al 1978 *Handbook on Physical and Chemical Properties of Oxides* ed G V Samsonov (Moscow: Metallurgiya) p 471 (in Russian)
- [70] Glang R 1970 *Handbook of Thin Film Technology* ed L I Maisell and R Glang (New York: McGraw-Hill) p 89
- [71] Voronov D L, Zubarev E N, Kondratenko V V, Penkov A V, Pershin Yu P, Ponomarenko A G, Artiukov I A, Vinogradov A V, Uspenskii Yu A and Seely J F 2002 *X-ray Lasers 2002: 8th Int. Conf. X-ray Lasers* (Aspen, CO) *AIP Conf. Proc.* **641** 575–82 (New York: AIP) ed J J Rocca et al
- [72] Jankowski A F, Saw C K, Walton C C, Hayes J P and Nilsen J 2004 *Thin Solid Films* **469–470** 372
- [73] Gautier J, Delmotte F, Rouilly M, Ravet M F, Bridou F, Jerome A, Giglia A and Nannarone S 2005 *Proc. SPIE* **5963** 59630X